Knl1 participates in spindle assembly checkpoint signaling in maize

Handong Su[a,1], Yang Liu[a,b,1], Chunhui Wang[a,b,1], Yalin Liu[a], Chao Feng[a], Yishuang Sun[a,b], Jing Yuan[a], James A. Birchler[c], and Fangpu Han[a,b,2]

[a]State Key Laboratory of Plant Cell and Chromosome Engineering, Institute of Genetics and Developmental Biology, Innovation Academy for Seed Design, Chinese Academy of Sciences, 100101 Beijing, China; [b]College of Advanced Agricultural Sciences, University of the Chinese Academy of Sciences, 100049 Beijing, China; and [c]Division of Biological Sciences, University of Missouri, Columbia, MO 65211-7400

Edited by Gregory P. Copenhaver, University of North Carolina at Chapel Hill, Chapel Hill, NC, and accepted by Editorial Board Member Joseph R. Ecker April 6, 2021 (received for review October 26, 2020)

The Knl1-Mis12-Ndc80 (KMN) network is an essential component of the kinetochore–microtubule attachment interface, which is required for genomic stability in eukaryotes. However, little is known about plant Knl1 proteins because of their complex evolutionary history. Here, we cloned the *Knl1* homolog from maize (*Zea mays*) and confirmed it as a constitutive central kinetochore component. Functional assays demonstrated their conserved role in chromosomal congression and segregation during nuclear division, thus causing defective cell division during kernel development when Knl1 transcript was depleted. A 145 aa region in the middle of maize Knl1, that did not involve the MELT repeats, was associated with the interaction of spindle assembly checkpoint (SAC) components Bub1/Mad3 family proteins 1 and 2 (Bmf1/2) but not with the Bmf3 protein. They may form a helical conformation with a hydrophobic interface with the TPR domain of Bmf1/2, which is similar to that of vertebrates. However, this region detected in monocots shows extensive divergence in eudicots, suggesting that distinct modes of the SAC to kinetochore connection are present within plant lineages. These findings elucidate the conserved role of the KMN network in cell division and a striking dynamic of evolutionary patterns in the SAC signaling and kinetochore network.

Knl1 | SAC | kinetochore | maize | cell division

The proper partitioning of chromosomes to daughter cells during mitosis and meiosis relies on the hierarchical kinetochore protein complex that assembles on the centromeres of chromosomes (1, 2). Detailed microscopy and biochemical studies have identified more than 100 kinetochore proteins from yeast to mammalian cells and have revealed the conserved bipartite structure of the kinetochore (3). The outer kinetochore Knl1-Mis12-Ndc80 (KMN) network physically connects the centromeric chromatin and the inner constitutive kinetochore–centromere-associated network to the spindle microtubules, which cooperate for faithful chromosome orientation and segregation during cell division (1, 4–6). The conserved spindle assembly checkpoint (SAC) signaling regulates the attachment of kinetochores and microtubules (KT–MT) and delays the progression of the cell cycle until all kinetochores are correctly attached (7–9). The KT–MT associations and their regulatory machineries are relatively conserved in eukaryotes. However, kinetochore proteins undergo frequent mutations and have coevolved in various ways with their interaction partners, leading to great diversity in kinetochore composition in eukaryotes (6, 10). The functional study of kinetochore compositions in plant species besides model organisms will be necessary to shed light on this intriguing complex during evolution.

Knl1 is one of the largest kinetochore components and plays important roles in the assembly of other kinetochore proteins and chromosomal congression during cell division in *Caenorhabditis elegans*, yeast, and human cells (11–17). As the "hub" of the kinetochore, Knl1 displays high levels of intrinsic disorder with many short linear motifs to coordinate multiple protein–protein interactions for microtubule attachment and activation of SAC signaling during the cell cycle (7, 18). At the N terminus of human Knl1, two KI motifs, KI1 and KI2, are identified with confidence only in vertebrates and interact with SAC components Bub1 and BubR1, respectively (Fig. 1*A*). The crystal structure reveals that some residues of the KI motifs form part of an alpha helix that runs parallel to the axis of the TPR domain of these proteins (16, 19, 20). Recent studies in yeast and humans have revealed that the Mps1-dependent, phosphorylated MELT repeats in Knl1 generate binding sites for SAC component Bub3 and promote the recruitment of Bub3–Bub1 and Bub3–BubR1 complexes to the kinetochore (21–24). The KI motifs were further found to be the enhancers of MELT modules in the recruitment of SAC signals in human Knl1 (25). However, the number of MELT repeats in Knl1 varies among species, and no MELT repeats and convincing KI motifs were detected in the plant Knl1 protein (Fig. 1*A*) (26). The questions then arise of how the SAC components interact with Knl1 in flowering plants, which have no explicit repeats, and what are the roles of plant Knl1 in regulating the spatial and temporal behavior of chromosomes during the cell cycle.

Significance

The spindle assembly checkpoint (SAC) signaling controls the attachments of kinetochores to spindle microtubules rigorously. However, how SAC proteins connect to the kinetochores is largely unknown in plants. Here, we identified the constitutive component of the central kinetochore protein Knl1 in maize and revealed a conserved function of Knl1 in cell division. A helical conformation with hydrophobic amino acids in the middle of a Knl1 protein was involved in the recruitment of an SAC protein, which is different from the Mps1-mediated phosphorylation of MELT modules that are described in yeast and mammalian cells. This region, detected in maize Knl1, is conserved in monocots but displays high divergence in eudicots, suggesting distinct kinetochore architectures with SAC signaling in plant lineages.

Author contributions: H.S., J.A.B., and F.H. designed research; H.S., Yang Liu, C.W., Yalin Liu, C.F., Y.S., and J.Y. performed research; H.S., Yang Liu, C.W., J.A.B., and F.H. analyzed data; and H.S., Yang Liu, J.A.B., and F.H. wrote the paper.

The authors declare no competing interest.

This article is a PNAS Direct Submission. G.P.C. is a guest editor invited by the Editorial Board.

[1]H.S., Yang Liu, and C.W. contributed equally to this work.

[2]To whom correspondence may be addressed. Email: fphan@genetics.ac.cn.

This article contains supporting information online at https://www.pnas.org/lookup/suppl/doi:10.1073/pnas.2022357118/-/DCSupplemental.

Published May 14, 2021.

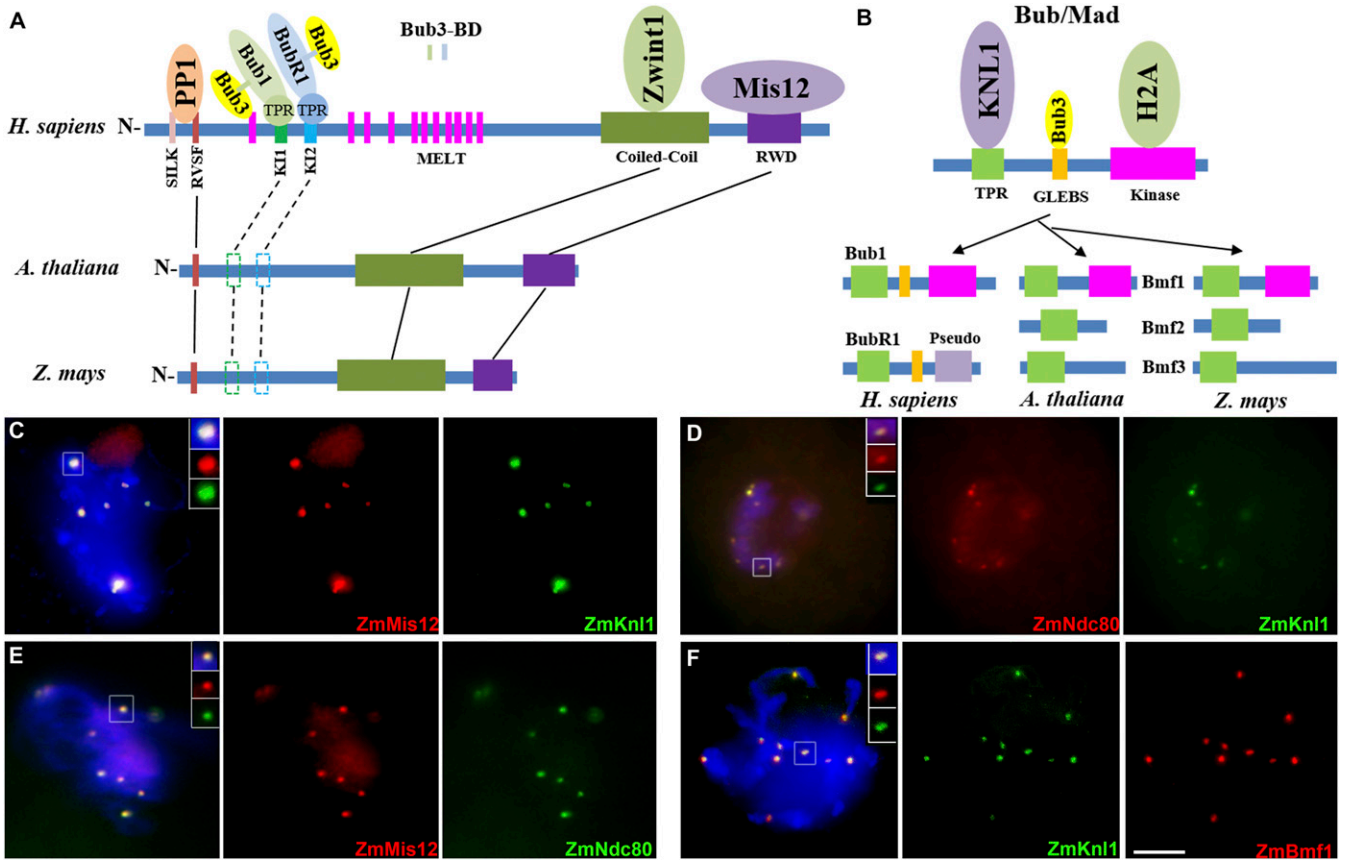

Fig. 1. Identification and annotation of the Knl1 homolog in maize. (*A*) Schematic diagram of Knl1 and SAC components in humans (*H. sapiens*), *Arabidopsis* (*A. thaliana*), and maize (*Z. mays*). Different-colored rectangles on human Knl1 represent the following: SILK and RVSF motif for PP1 binding domain; MELT repeats and KI1 motif for Bub3–Bub1 complex binding; KI2 motif for Bub3–BubR1 complex binding; coiled-coil domain for Zwint1 binding; and RWD domain for Mis12 complex binding. Ovals on Bub1 and BubR1 represent the TPR domains. Rectangles on Bub1 and BubR1 represent the Bub3-binding domain. Only RVSF, coiled-coil, and RWD domains are present in *Arabidopsis* and maize Knl1. The dotted lines and virtual boxes indicate there are no KI motifs in plant Knl1. (*B*) Model for evolution of the Bub/Mad family protein in humans, *Arabidopsis*, and maize. Some functional domains were shown with different-colored rectangles in the presumed ancestral Bub1/Mad3 protein. TPR domain is for Knl1 binding, GLEBS motif is for Bub3 binding, and a kinase domain is for histone H2A phosphorylation. A pseudokinase domain with a gray rectangle was shown in human BubR1. (*C–E*) Colocalization of KMN network components on maize leptotene and pachytene chromosomes: ZmMis12 (red) and ZmKnl1 (green) (*C*); ZmNdc80 (red) and ZmKnl1 (green) (*D*); and ZmMis12 (red) and ZmNdc80 (green) (*E*). (*F*) Colocalization signals of ZmKnl1 (green) and ZmBmf1 (red) in maize pachytene chromosomes. The *Insets* indicate a higher-magnification view of colocalization signals of different proteins. Chromosomes stained with DAPI are shown in blue. (Scale bar, 10 μm.)

Plant SAC components were first identified in *Arabidopsis* (27, 28), and subsequent studies reveal they share conserved functions but exhibit different architectures with their counterparts compared with animals and yeast (29, 30). Molecular intricacies of SAC signaling in plants seems to be highly divergent from the system in vertebrate and fungal lineages. For example, the reshuffled and redistributed domains from the presumed ancestral Bub1/Mad3 with two independent duplication events result in three Bub1-type paralogs in plants, referred to as the Bub1/Mad3 family protein (Bmf1, Bmf2, and Bmf3), which is different from animals and yeast with two Bub1-type paralogs (Bub1, BubR1, or Mad3, Fig. 1*B*) (26, 29). *Arabidopsis thaliana* Bmf1 (AtBmf1) shows constant kinetochore signals during the cell cycle, AtBmf2 is not present in the kinetochore, and only AtBmf3 displays a typical dynamic kinetochore distribution when compared to other species (29). Moreover, three Bub3 paralogs in *Arabidopsis* were identified and were shown not to be localized in the kinetochore but to function in microtubule organization during cytokinesis (29, 31). The Gle2-binding site (GLEBS) in Bub1 and BubR1, which are involved in the interaction with Bub3 in human cells, has been lost in plant BMF proteins (9, 32). These results indicate that the protein sequences and functions of plant SAC have occurred with divergence, compared with that of animals and yeast. Therefore, the kinetochore receptor of SAC components and their binding patterns with kinetochores need further research in plants.

Mis12 and Ndc80, the core proteins of the KMN network, have previously been found to localize in the kinetochore in maize (33, 34). Here, we cloned a *Knl1* homolog from maize, and the mutant analysis demonstrated a conserved role played by this protein during plant cell division, as well as in early endosperm development. Evolutionary and functional analyzes further shed light on an intriguing pattern of molecular evolution models between Knl1 and SAC components in plants.

Results

Identification and Annotation of the Knl1 Homolog in Maize. A recent paper reported Knl1 in moss *Physcomitrella patens* was localized to the kinetochore (35). Here, we used the protein sequence as a query to Basic Local Alignment Search Tool (BLAST) the National Center for Biotechnology Information (NCBI) protein database and cloned the *Knl1* homolog from maize. The candidate gene (Zm00001d046545) encodes a 1,065 amino acid (aa) polypeptide. RT-PCR revealed that this gene is highly expressed in young tassel and root tissues, which have high cell division indices, whereas it is expressed at significantly lower

levels in leaves, shoots, and older tissues (*SI Appendix*, Fig. S1*A*); this expression pattern is consistent with its kinetochore function during cell division. We performed dual immunostaining using the corresponding antibodies in wild-type (WT) maize pollen mother cells to detect the signals of the KMN network on meiotic-stage chromosomes. ZmNdc80 and ZmMis12 colocalized with this protein in zygotene- or pachytene-stage chromosomes, respectively (Fig. 1 *C* and *D*), when ZmNdc80 and ZmMis12 were also spatially associated (Fig. 1*E*). Furthermore, the colocalized signals of ZmKnl1 and ZmBmf1 might suggest the interaction with SAC signaling (Fig. 1*F*). Protein domain annotations indicate that the *N* and C termini contain conserved RVSF and coiled-coil domains, respectively, which are typical structural features of human Knl1 protein (Fig. 1*A* and *SI Appendix*, Fig. S1*B*). Conserved RWD domains were also determined in the C terminus tail using a hidden Markov model (HMM) (Fig. 1*A*) (36). However, we failed to detect other conserved motifs or domains in plant Knl1 proteins, including the SILK motif and convincing KI motifs at the N terminus, and the MELT repeats in the middle region (Fig. 1*A*). Protein disorder prediction identified a 630 aa region from the N terminus and several small regions in the C terminus that are intrinsically disordered, which is consistent with the structure of the human Knl1 protein (*SI Appendix*, Fig. S1*C*). Taken together, these results demonstrate that the Knl1 protein may act as a conserved kinetochore scaffold, with a divergence in plants.

To further investigate the evolutional history of Knl1, we built a phylogenetic tree of Knl1 among different species. The protein sequences of Knl1 were obtained via BLAST in the GenBank database or the HMM profile (37, 38). We identified Knl1 homologs from different plant lineages, including 44 eudicots, 18 monocots, 3 bryophytes, and 4 green algal species. *Amborella trichopoda*, at the base of the angiosperm tree (39), was also added to the analysis. Other Knl1 proteins from metazoa and fungi were obtained from the published resources (10, 26, 36). Multiple sequence alignment from various species reveals Knl1 proteins display poor overall sequence conservation (Dataset S1), indicating that Knl1 proteins diverged extensively during evolution. The phylogenetic tree shows that Knl1 from angiosperms is separated from that of fungi and metazoa. However, the Knl1s from chlorophyta and bryophyte belong to the fungal grade of Knl1. This may be due to fungal, green algal, and bryophytes Knl1s remaining more similar to the ancestral eukaryotic state, while land plant Knl1 diverged more extensively. Furthermore, independent branches evolved among eudicots and monocots, and Knl1 from *A. trichopoda* was situated in the node of the branch, implying the roles of Knl1 among different plant lineages may have differentiated (*SI Appendix*, Fig. S2). These results further confirmed the notion that kinetochore compositions diverged extensively during the evolution of eukaryotes, despite its conserved and essential cellular functions (10).

TPR Domains of ZmBmf1/2 Mediates the Interactions with ZmKnl1. We reasoned that the loss of some motifs in plant Knl1s that are conserved in human and yeast Knl1 might have led to changes in the interaction patterns between Knl1 and SAC proteins in maize. We therefore investigated whether ZmKnl1 interacts with SAC components using the yeast two-hybrid (Y2H) system. As the yeast cells with a full-length pGAD-Knl1 construct cannot grow on permissive media (SD/−Leu/−Trp), we used the Knl1-N construct to perform Y2H with different SAC proteins (as shown in Fig. 2*A*, this construct shows interaction with Bmf1/2). We found that ZmKnl1 interacted with full-length ZmBmf1 and ZmBmf2 in the Y2H system (Fig. 3 *A* and *B*). As the construct pGBK-ZmBmf3 shows self-activation, we built a pGBK-ZmKnl1-N construct, which also self-activates. Therefore, we generated several truncated pGBK-ZmKnl1 constructs covering the full-length ZmKnl1 and found that no interactions were detected with ZmBmf3 using these constructs in the Y2H assay (Fig. 3*C*), perhaps because the neofunction of ZmBmf3 affects its interaction with ZmKnl1. No interaction was detected between ZmKnl1 and ZmBub3 using the overlapping *N* or C terminus of ZmKnl1 (*SI Appendix*, Fig. S3*A*), whereas these proteins directly interact in mammalian cells and yeast (24, 40). Furthermore, we failed to detect interactions between ZmBmf1/2/3 and ZmBub3 (*SI Appendix*, Fig. S3*B*), which is consistent with the finding that plant BMF proteins lack the Bub3-binding domain (9, 29, 30).

As the TPR domain of Bub1 and BubR1 is essential for their interaction with Knl1 in human and yeast cells (15, 16, 19, 20), the conserved TPR domain was detected in the N terminus of ZmBmf1/2. We further investigated their interactions with ZmKnl1 using the Y2H assay (Fig. 3*D*) and generated a variety of constructs using the complete ZmBmf1 protein and truncation proteins containing the ZmBmf1–N terminus or ZmBmf1–C terminus. ZmBmf1-N, which harbors the TPR motif, interacts with ZmKnl1, as did the full-length ZmBmf1. By contrast, ZmBmf1-C failed to interact with ZmKnl1 (Fig. 3*A*, tracks two to three). The integral TPR domain contains three TPR repeat units (41). Removing either TPR repeat unit of ZmBmf1 will impair the interaction with ZmKnl1 (Fig. 3*A*, tracks four to five). To further verify that the TPR domain of ZmBmf1 is required for its interaction with ZmKnl1, we constructed several substitution mutants at conserved amino acids to perform Y2H. These mutations from the TPR domain (W-A, L-A, GMF-AGL, A-D, and V-G) of ZmBmf1 abolished its interaction with ZmKnl1 (Fig. 3*A*, tracks six to eight and *SI Appendix*, Fig. S3*C*). These sites are required for the interaction with Knl1 in human cells and yeast, and crystal structural analysis has confirmed that these impaired interactions are due to the disruption of stabilizing interactions with Knl1 and not as the result of complete misfolding of the protein (20, 42, 43). A similar result was obtained for the interaction of ZmBmf2 with ZmKnl1 using the truncation and mutation assays (YRFL-ARFA, QIG-AGL, A-D, and I-G) (Fig. 3*B* and *SI Appendix*, Fig. S3*D*). However, we found that the same mutation on the conserved residue (W-A) on the TPR domain of ZmBmf2 has no effect on the interaction with ZmKnl1 (Fig. 3*B*, track six), suggesting that ZmKnl1 recognizes ZmBmf1 residues differently from that of ZmBmf2. Taken together, these results reveal that the TPR domains of ZmBmf1/2 are essential for their association with ZmKnl1.

A Helical Conformation with Hydrophobic Amino Acids in the Middle Region of Knl1 Participates in BMF Recruitment in Maize. To further investigate how ZmKnl1 recognizes ZmBmf1/2, we mapped its binding domain using a series of overlapping ZmKnl1 truncations (Fig. 2*A*). Knl1-N (spanning aa 1 to 771) and Knl1-C (spanning aa 167 to 1,065) interacted with ZmBmf1/2 in a Y2H assay, indicating that the middle region of Knl1 (Knl1-M) interacts with both proteins (Fig. 2*B*, top three tracks). To determine the nature of the Knl1-M domain, we performed extensive Y2H analyses using truncation fragments of Knl1-M. The Knl1-M was truncated into three fragments (Knl1-M1 to Knl1-M3), as shown in Fig. 2*A*. Only Knl1-M3 interacted with both ZmBmf1 and ZmBmf2, whereas Knl1-M1 and Knl1-M2 failed to interact with either protein (Fig. 2*B*, tracks four to six). We then truncated Knl1-M3 into five small parts. Whereas Knl1-M4 to Knl1-M7 did not interact with ZmBmf1 or ZmBmf2, the Knl1-M8, that consisting of Knl1-M6 and the distal part of Knl1-M7, interacted with both proteins (Fig. 2*B*). Luciferase complementation imaging assays in *Nicotiana benthamiana* leaves revealed that the coexpression of ZmBmf1/2-NLUC (N-terminal domains of LUCIFERASE) and ZmKnl1-M8-CLUC (C-terminal domains of LUCIFERASE) displayed a strong luciferase activity, indicating a specific interaction of ZmKnl1-M8 with ZmBmf1 and ZmBmf2 but not with ZmBmf3 (Fig. 2*C*). These results suggest that the Bmf1/2 recruitment region comprises 145 aa in

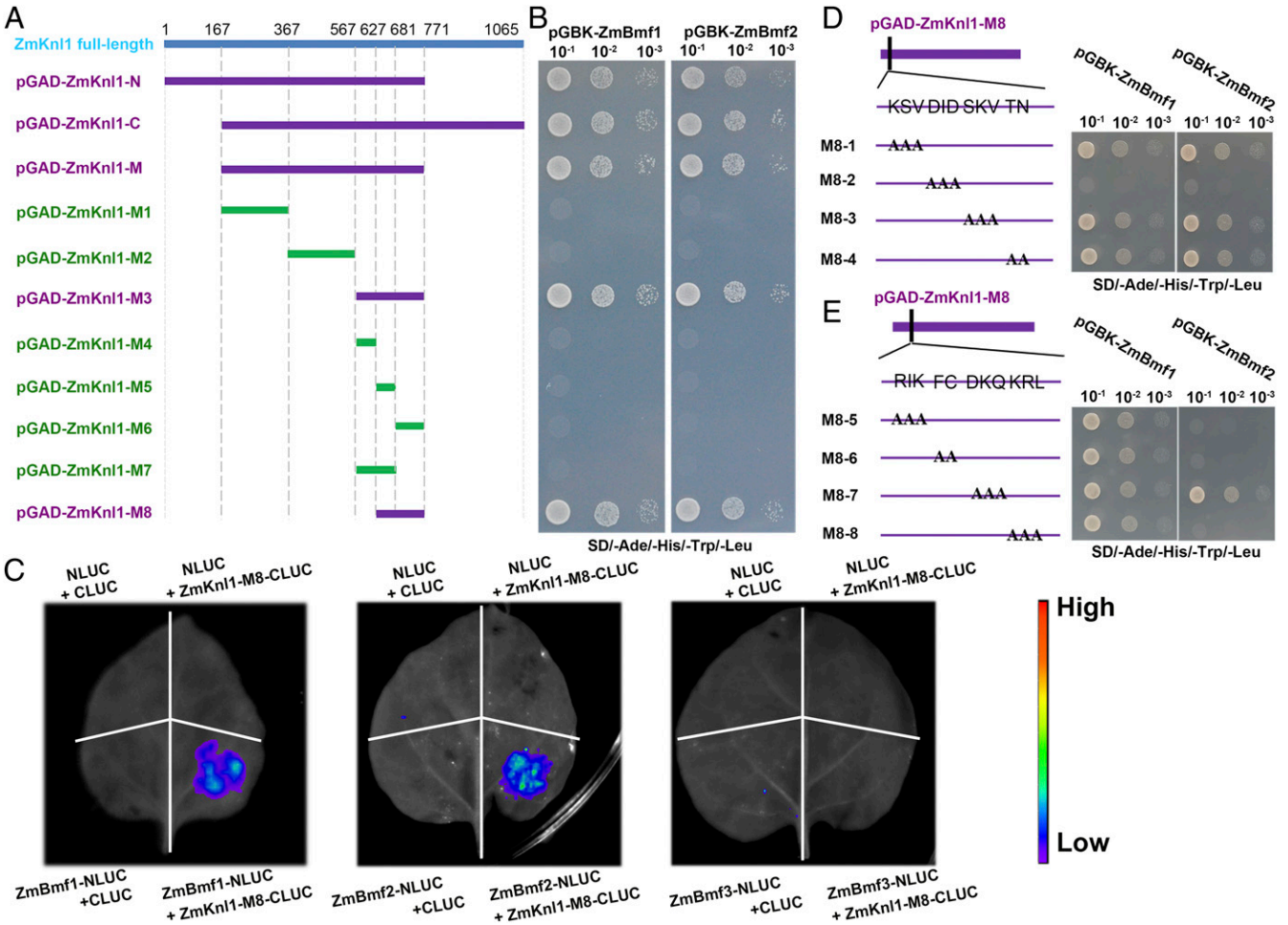

Fig. 2. Identification of the BMF binding domain in ZmKnl1. (*A*) Schematic representation of the ZmKnl1 truncations used to define the ZmBmf1/2 binding domain. Eight truncated constructs of ZmKnl1 (M1 to M8) were produced. Blue indicates full-length ZmKnl1 proteins. Green indicates no Y2H interaction. Purple indicates Y2H interaction. (*B*) Y2H interactions between truncated ZmKnl1 variants and ZmBmf1 (*Left* three) or ZmBmf2 (*Right* three). (*C*) Luciferase complementation imaging assay of the interaction between ZmKnl1-M8 and ZmBmf1/2/3. Fluorescence signal intensities represent their interaction activities. (*D* and *E*) Schematic representation of ZmKnl1 substitution constructs used to define the ZmBmf1/2-binding domain. Y2H interaction was conducted between substituted ZmKnl1 variants and ZmBmf1/2. The sequential residues in this region were replaced with As.

the middle of the Knl1 protein, spanning residues 627 to 771 in maize (ZmKnl1$^{627–771}$).

To characterize the BMF recruitment region in ZmKnl1, we predicted the secondary structure with Raptorx server (44), and three alpha helices with two bulky hydrophobic domains were detected in this region (*SI Appendix*, Fig. S4 *A* and *B*). To determine whether the hydrophobic amino acids are essential for the interaction with ZmBmf1/2, we performed Y2H experiments using a series of ZmKnl1 mutant proteins, in which most of the residues were substituted with alanine (A) via site-directed mutagenesis in the Knl1-M8 construct. When amino acid residues DID in the first hydrophobic domain with an alpha helix were replaced by AAA, ZmKnl1 failed to interact with ZmBmf1/2. Mutations at other sites (KSV-AAA, SKV-AAA, and TN-AA) had no effect on its interaction with ZmBmf1 or ZmBmf2 (Fig. 2*D*). We found that the replacement of second hydrophobic domains (RIK, FC, and KRL) with As abolished its interaction with ZmBmf2 but did not affect its interaction with ZmBmf1 (Fig. 2*E*), suggesting that the mechanism by which ZmKnl1 recognizes ZmBmf1 is subtly different to that of ZmBmf2, and at least another segment of ZmKnl1 is involved in the interaction with ZmBmf2 protein. This is consistent with the results that particular constructs containing the hydrophobic amino acids show no binding with ZmBmf1/2 (Fig. 2*A*, M5 and M7). Furthermore, a coiled-coil region was detected in the last part of the 145 aa region (*SI Appendix*, Fig. S4*A*). The mutations of these conserved residues in the coiled-coil region have no effect on the interaction with ZmBmf1/2 (*SI Appendix*, Fig. S4*C*). These results indicate that the BMF recruitment region in ZmKnl1 contains a helical conformation with hydrophobic amino acids, and they may form a complementary hydrophobic interface with the TPR domain of BMF proteins, as in vertebrates.

However, when we compared the regions between different plant lineages, the BMF recruitment region detected in maize was found with differentiations in eudicots, such as *Arabidopsis*, soybean (*Glycine max*), and *Brassica* species (*SI Appendix*, Fig. S4*A*). The mutations on the highly conserved amino acids between eudicots and monocots in the last part of 145 aa region have no effect on the interaction with ZmBmf1/2 (*SI Appendix*, Fig. S4*C*), suggesting that the conserved parts in the 145 aa region of Knl1 between monocots and eudicots are not associated with interaction to ZmBmf1/2. Only the specific residues in the diverged domain influence the interaction with ZmBmf1/2 (Fig. 2 *D* and *E*). These results suggest that different mechanisms evolved to recruit BMF proteins to kinetochore between eudicots and monocots.

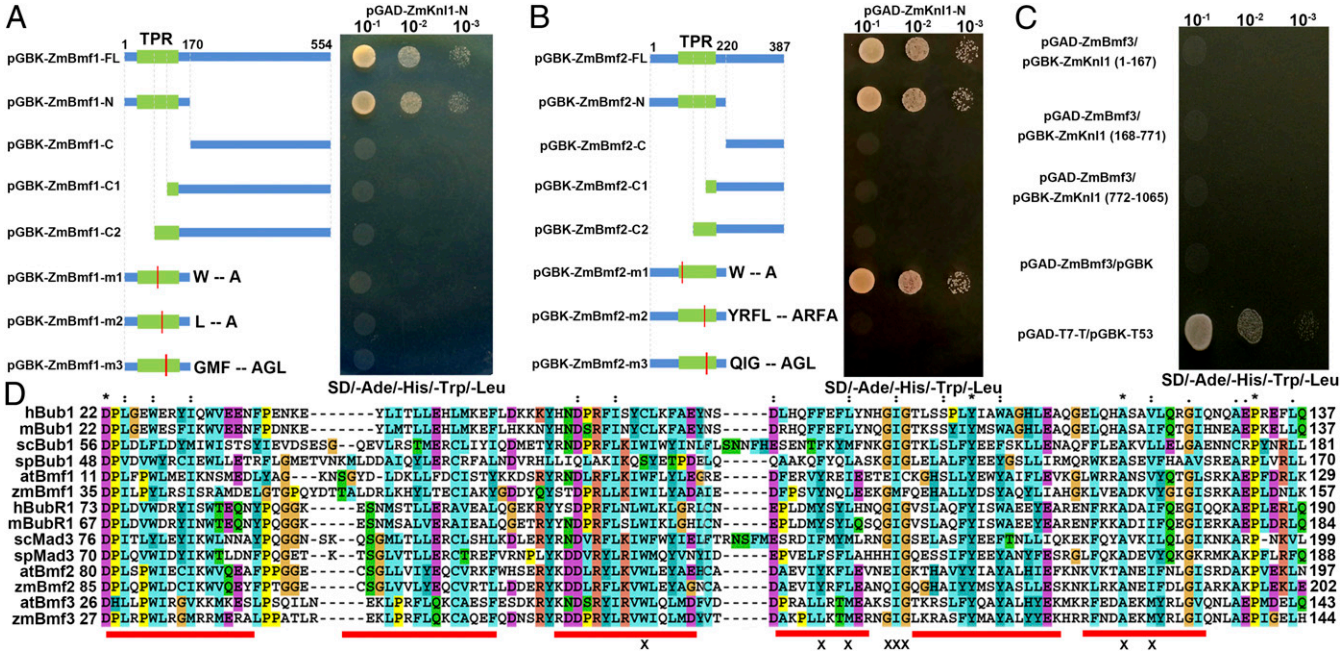

Fig. 3. The TPR domains of ZmBmf1 and ZmBmf2 are essential for binding with ZmKnl1. (*A–C*) Schematic representations of the truncations and mutations of BMF proteins used to define the Knl1 binding domain (*Left*). Y2H system of ZmKnl1 with different BMF constructs (*Right*): ZmBmf1 (*A*), ZmBmf2 (*B*), and ZmBmf3 (*C*). The TPR motif is marked in green. Red indicates residues altered in the substitution mutants, as depicted in *D*. FL is full length; N is N terminus containing the TPR domain; C is C terminus without the intact TPR domain; C1 is C terminus without one TPR repeat unit; and C2 is C terminus without two TPR repeat units. Yeast cells at various dilutions were grown on selective (SD/−Trp/−Leu/−Ade/−His) media. (*D*) Multiple sequence alignment of the TPR domains of Bub1/Mad3 homologs from human (h), mouse (m), *Saccharomyces cerevisiae* (sc), *Schizosaccharomyces pombe* (sp), *Arabidopsis* (at), and maize (zm). The asterisks at the top of the alignment indicate completely conserved residues, and the colons and single dots indicate highly and moderately conserved residues, respectively. The red line indicates the alpha helix within the TPR domain. X indicates residues altered in the substitution mutants.

Knl1 Is a Constitutive Component of the Central Kinetochore during the Cell Cycle. We performed immunofluorescence microscopy using monoclonal antibodies to detect ZmKnl1 signals in meristem cells from root tips of a YFP-CENH3 transgenic maize line during the cell cycle and to compare the distribution pattern of ZmKnl1 with that of CENH3. ZmKnl1 was firstly detected in the interphase of somatic meristem cells (*SI Appendix*, Fig. S5*A*), and the antiserum identified all 20 kinetochores labeled with CENH3 signals in somatic nuclei throughout the cell cycle (*SI Appendix*, Fig. S5). ZmKnl1 signals were located in front of the kinetochore after anaphase (*SI Appendix*, Fig. S5 *C* and *D*), as sister chromatid kinetochores were connected with spindle microtubules to separate the sister chromatids.

We then examined the localization of ZmKnl1 in the kinetochore of WT pollen mother cells. ZmKnl1 signals were readily observed on all kinetochores in meiotic cells during all stages of the cell cycle (Fig. 4). When chromosomes condensed and began to pair during the leptotene and early zygotene stages, Knl1 appeared as distinct single (paired) or doubled (unpaired) spots (Fig. 4 *A–C*). ZmKnl1 stained brightly in chromosomes later in the cell cycle during pachytene, when all kinetochores were paired and contained four chromatid kinetochores (Fig. 4*C*). ZmKnl1 signals were clearly localized to kinetochores throughout meiosis II until telophase II, as well as in cells that had completed meiosis (i.e., tetrads) (Fig. 4 *F–H*). ZmKnl1 signals connected with microtubules during metaphase I and metaphase II (*SI Appendix*, Fig. S6). The consistent signals of ZmKnl1 on kinetochores indicate that Knl1 is constitutively present in maize, as previously reported for ZmNdc80 (33).

CRISPR/Cas9-Mediated Knockout of ZmKnl1 Cause Defects in Chromosomal Congression during Mitosis. To further explore the role of ZmKnl1 in chromosome segregation, we created knockout mutants of ZmKnl1 using the *dmc1* promoter-controlled (DPC) CRISPR/Cas9 system, which is highly efficient for genome editing in maize (45). For the targeting site of ZmKnl1, we selected a *Pvu*-II recognition site within the second exon of this gene (*SI Appendix*, Fig. S7*A*). We transformed the construct into immature maize Hi-II embryos via *Agrobacterium tumefaciens*–mediated transformation and obtained four bialaphos-resistant calli (transgene positive) and 20 regenerated plantlets. The regenerated seedlings exhibited a high mutation ratio, as determined by PCR restriction enzyme (PCR-RE) digestion assay (*SI Appendix*, Fig. S7*B*). Various types of mutations were present in *zmknl1*, as revealed by Sanger sequencing (*SI Appendix*, Fig. S7*C*). Sanger sequencing of transgenic seedlings #7, #12, and #19 indicated that they were likely mosaic mutants with two or three mutated alleles, respectively (26/25/12/3/1 bp deletion or 1 bp insertion). Transgenic seedlings with high mutation ratios grew slowly and did not survive for more than 2 wk (*SI Appendix*, Fig. S7*D*).

To better understand the reasons of the growth defects in these lines, we obtained root-tip cells from the seedling during early growth, fixed them, and stained them with DAPI. Chromosome morphology in the *ZmKnl1* mutants was similar to that of the control through prophase (Fig. 5 *A* and *B*). However, while the chromosomes of the control were well aligned at the equator of the cell in metaphase (Fig. 5*C*), about 33.3% of cells (n = 36) in the *ZmKnl1* mutants showed perturbed chromosome congression, with one to two chromosomes that failed to align (Fig. 5*D*). These results indicate that ZmKnl1 is required for mitotic chromosomal congression, which is consistent with the findings that ZmKnl1 regulates chromosome alignment and segregation in human cells (16, 17).

ZmKNL1 Deficiency Is Correlated with Defective Kernel Development. Using the ZmKnl1 protein sequence as a query, we searched the

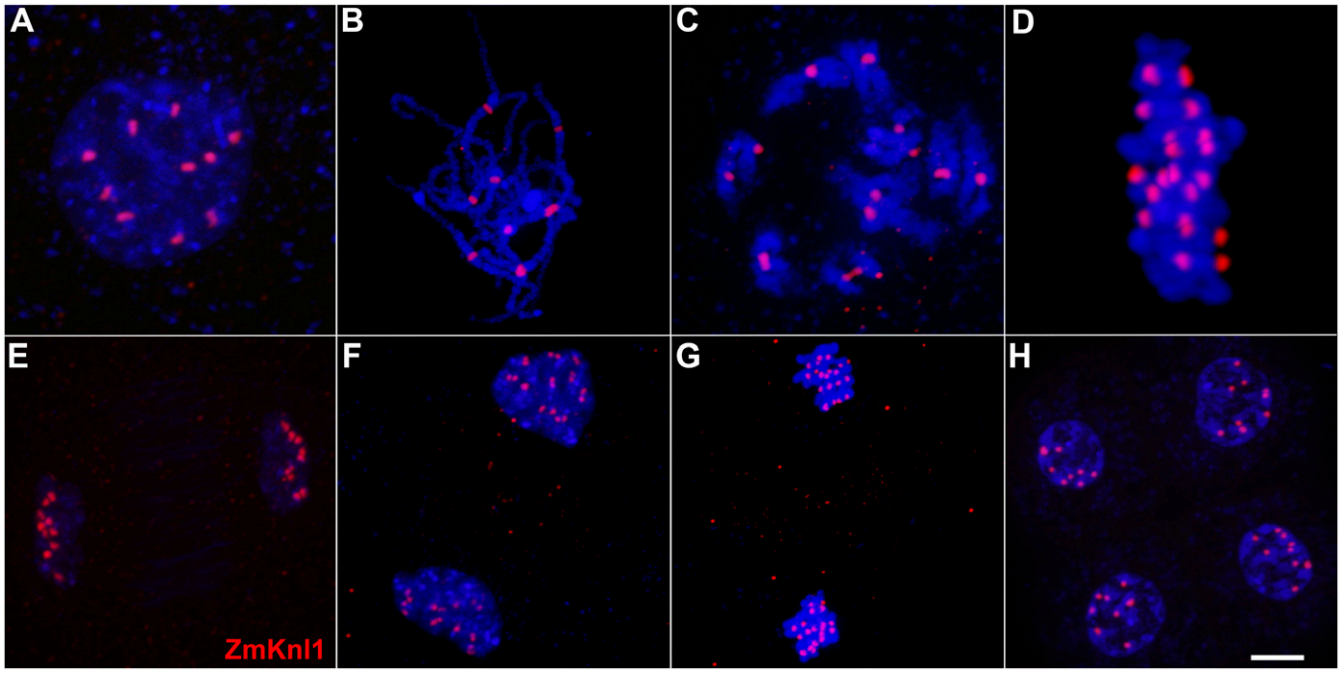

Fig. 4. Distribution of ZmKnl1 signals in WT maize meiocytes: leptonema (*A*), pachynema (*B*), diakinesis (*C*), metaphase I (*D*), Telophase I (*E*), prometaphase II (*F*), metaphase II (*G*), and quartets (*H*). ZmKnl1 signals are shown in red. DAPI-stained chromosomes are shown in blue. (Scale bar, 10 μm.)

maizeGDB UniformMu resource (https://www.maizegdb.org/uniformmu) and located a *UFMu-06469* line carrying a Mutator (Mu) insertion. The mutant was crossed with plants in the W22 genetic background. Genotyping showed that a Mu transposon is inserted in the first exon of the *zmknl1* gene after the ATG start codon (Fig. 6*A*). Some of the mature kernels were small and shrunken (*SI Appendix*, Fig. S8*A*). The F2 ears of heterozygous plants exhibited a 3:1 segregation ratio of WT to mutant kernels (*SI Appendix*, Fig. S8*B*), indicating that *UFMu-06469* harbors a recessive mutation. We extracted genomic DNA from small and normal kernels without removing the endosperm. Genotyping using the prime pair F+R/R+Mu revealed that the small kernels were homozygous (*SI Appendix*, Fig. S8*C*). At 14 d after pollination (DAP), homozygous *knl1* kernels were small and appeared collapsed (Fig. 6 *B* and *C*). RT-PCR showed that Knl1 is not expressed in small kernels (*SI Appendix*, Fig. S8*D*). At maturity, the 100-seed weight of mutant seeds was significantly reduced to a level of only 1.2% that of the WT (*SI Appendix*, Fig. S8*E*; $P < 0.01$). The homozygous mutant seeds failed to germinate (Fig. 6*D*). No homozygous Knl1 mutant survived, indicating that normal development cannot occur in the absence of Knl1. Chromosome spreads were examined in the WT and *zmknl1* endosperm cells at 14 DAP. Chromosome bridges (62.5%, n= 24) during anaphase were easily observed in *zmknl1* endosperm (Fig. 6*E*), suggesting that the deficiency of ZmKNL1 causes mitotic defects in endosperm cells.

To further understand the basis of the phenotypic defects of the *zmknl1* mutant, we performed RNA sequencing (RNA-Seq) of mutant and WT kernels at 14 DAP with two biological replicates (*SI Appendix*, Fig. S8*F*). In total, 555 significantly differentially expressed genes (DEGs) were identified (*q-value* < 0.05, log2 [fold change] > 1.5), including 317 down-regulated and 238 up-regulated genes (*SI Appendix*, Fig. S8*G* and Dataset S2). We functionally analyzed 432 of these DEGs using the Gene Ontology (GO) analysis. The kinetochore genes, including SAC, Ndc80, and Mis12 components, were not in the list of DEGs, suggesting that the Knl1 deregulation has no effect on the expression of other kinetochore genes. The enriched GO terms mainly included metabolic process (GO:0008152), response to stimulus (GO:0050896), anatomical structure development (GO:0048856) (multicellular organism development, developmental process involved in reproduction, reproductive process, system development, seed development, fruit development, postembryonic development, and reproductive structure development), and monocarboxylic acid metabolic process (GO:0032787) (organic acid biosynthetic process, oxoacid metabolic process, carboxylic acid biosynthetic process, carboxylic acid metabolic process, and fatty acid biosynthetic process) (*SI Appendix*, Fig. S8*H* and Dataset S3), which were previously shown to be involved in maize endosperm development (46). Taken together, these results suggest the loss of function of ZmKnl1 affects mitotic cell division during early endosperm development and triggers a stress response and the corresponding metabolic reactions.

Discussion

Knl1 is a highly divergent protein widely conserved among eukaryotes. The function of plant Knl1 has not been properly studied to date. Here, we cloned the Knl1 gene from maize and present cytological and evolutionary data about this protein in plant lineages. The spatial and cellular localization patterns of Knl1 signals overlapped with those of Mis12 and Ndc80 in maize, which are other established components of the KMN complex (Fig. 1 *C*–*E*). Although the overall sequence similarity of Knl1 proteins across species is very low, functional analysis revealed that Knl1 is essential for proper chromosome congression and segregation during cell division (Figs. 5 and 6), which is consistent with findings in human cells (16, 17). The mutation of a motor protein was recently found to affect mitotic division during early endosperm development in maize, yielding plants with various kernel sizes (47). The deficiency of Knl1 likely impairs kinetochore function, leading to abnormal chromosome behavior during cell division in early endosperm development, subsequently eliciting a stress response and corresponding metabolic reactions and ultimately resulting in defective kernels.

When we investigated the mechanism of how Knl1 is involved in SAC signaling in plant systems, other aspects were found.

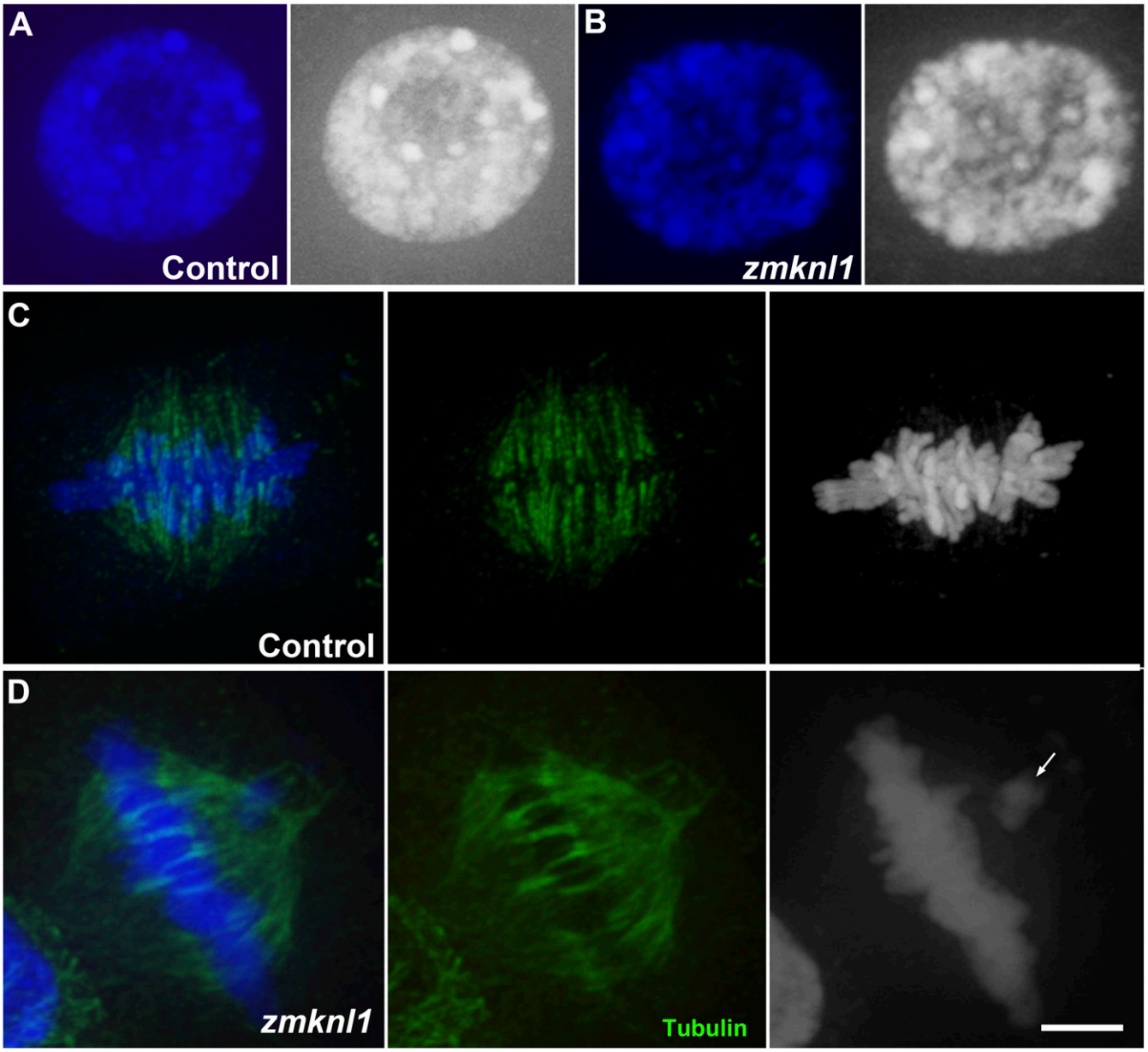

Fig. 5. Knockout of ZmKnl1 by CRISPR/Cas9 leads to defects in chromosome congression during mitosis. (*A* and *B*) Prophase cells from the root tips of the control (*A*) (the transgene-negative lines were treated as the control) and a *zmknl1* knockout mutant (*B*). (*C* and *D*) Representative chromosome congression in root-tip meristem cells during early growth in the control (*C*) and *zmknl1* knockout mutant (*D*). Arrows indicate unaligned chromosomes. Tubulin signals are shown in green. DAPI-stained chromosomes are shown in blue. (Scale bar, 10 μm.)

ZmBmf3 lost its interaction with ZmKnl1, and only ZmBmf1 and ZmBmf2 retained the interactions with ZmKnl1 (Fig. 3). ZmBmf1 shows a dynamic kinetochore localization during the cell cycle, of which the signals accumulate at the kinetochore in interphase, and signal intensity increases before metaphase and disappeared from the kinetochore at anaphase (9). The results were similar for the dynamic localization of Bmf1 protein in rice, another monocot species (48). There have been no reports of the localization of Bmf2/3 in maize and rice. We propose that the recruitment of kinetochore localization of BMF proteins might be related to the Knl1 pathway. Both of the plant BMF proteins contain the TPR domain, as in humans. The mutational analysis at the conserved corresponding residues of the TPR domain between ZmBmf1 and ZmBmf2 (W-A) suggests ZmKnl1 recognizes TRP domains in different manners (Fig. 3). Therefore, sequence variations on the TPR domains at ZmBmf1/2 and ZmBmf3 may result in the lost interaction with Knl1.

The MELT repeats were lost in plant Knl1 (Fig. 1*A*), suggesting that an alternative pathway might exist for the interaction with SAC proteins. The kinetochore localization of SAC components' BMF proteins in *mps1* mutants is identical to that in WT *Arabidopsis*, further indicating that the Mps1-mediated phosphorylation process is dispensable for recruiting SAC components to the kinetochore in plants (29). Here, we identified 145 aa in the middle region of ZmKnl1 that interact with ZmBmf1/2 (Fig. 2). Furthermore, a comparison of protein sequences and experimental analysis revealed that the hydrophobic amino acids with alpha helix conformation in the 145 aa region involves its interaction with ZmBmf1/2, and the mechanisms differ subtly on how ZmKnl1 recognizes ZmBmf1 and ZmBmf2 (Fig. 2). Furthermore,

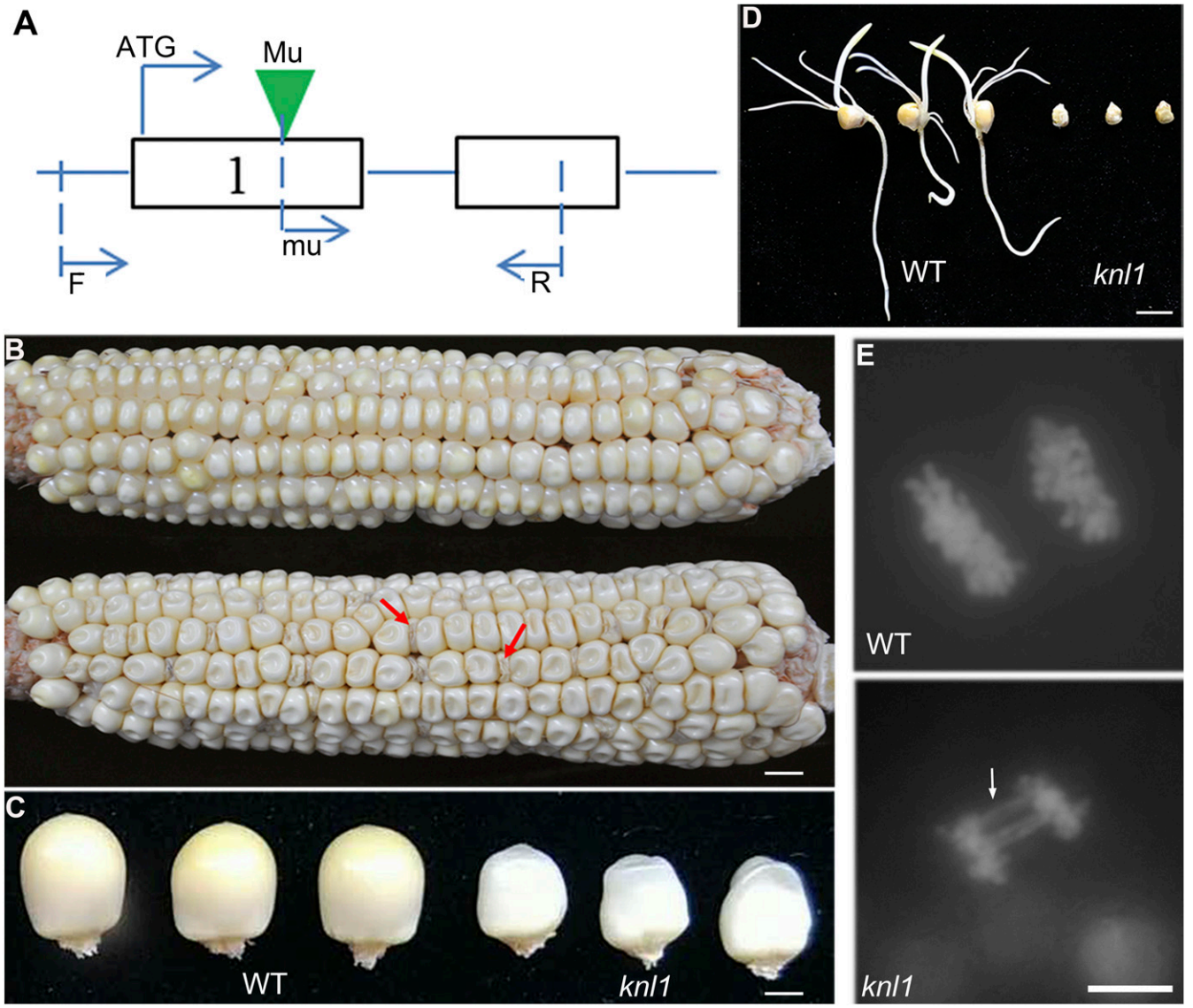

Fig. 6. ZmKNL1 Mu–insertion mutants display defective kernel development. (*A*) The Mu insertion in UFMu-06469 is located in the first exon of *zmknl1*. (*B*) Mature ear of a heterozygous *zmknl1* mutant. Arrow indicates a homozygous *UFMu-06469* (*zmknl1*) kernel. Red arrowheads indicate homozygous *zmknl1* kernels. (Scale bar, 1 cm.) (*C*) WT (*Left* three) and *zmknl1* (*Right* three) kernels at 25 DAP. (*D*) Comparison of germination in three WT (*Left*) and three *zmknl1* (*Right*) seeds at 5 d after germination. (Scale bar, 1 cm.) (*E*) The chromosome behavior of endosperm cells in the WT and *zmknl1* at 14 DAP at anaphase. The lagging chromosomes in the mutant are indicated by arrows. (Scale bar, 10 μm.)

the BMF recruitment region detected in maize shows significant variation in eudicots (*SI Appendix*, Fig. S4). We mutated the relatively conserved amino acids in the 145 aa region between monocots and eudicots, and these mutations show no effect on the interaction with ZmBmf1/2, suggesting that the conserved residues in this region between monocots and eudicots are not involved with the interaction with the BMF proteins. Recently, a MELT-like motif was predicted at the N terminus of Knl1 in all flowering plants, which was not involved in the 145 aa region of ZmKnl1 (49). This MELT-like motif may participate in the recruitment of BMF proteins in eudicots. These results suggest that different mechanisms exist for the connection of the SAC to kinetochores in flowering plants, and they need further studies in other plant systems.

The reason for the high degree of divergence with Knl1 proteins (rather than Ndc80 or Mis12 proteins) among species is currently unclear. Perhaps the intrinsically disordered nature of Knl1 provides a greater interaction surface and local conformational flexibility for the binding of multiple proteins (50–52). Comparative genomics of the kinetochore network in eukaryotes revealed that various kinetochore components have coevolved (10). The rapid evolution of plant Knl1 proteins might have induced the corresponding evolution of their partner proteins, thus mediating the emergence of new functions for these proteins or vice versa. Bub3 does not interact with Knl1 and Bmf1/2/3 in maize (*SI Appendix*, Fig. S3), suggesting that the role of Bub3 might have diverged in plants. Perhaps Bub3 is not involved in the checkpoint mechanism in plants, leading to the loss of interaction with the kinetochore scaffold protein Knl1. Conversely, perhaps the divergence of the Knl1 protein in plants has led to the loss of interaction with some SAC proteins and ultimately led to the loss of SAC function for Bub3. The plant SAC checkpoint system is involved in various activities, in addition to regulating chromosome segregation, such as various cellular and developmental processes (30). A recent study in *Arabidopsis* revealed that plant Bub3 functions in MAP65-3–dependent microtubule reorganization

during cytokinesis (31). The cell-cycle–dependent kinetochore localization of Bub3 signals have been observed during mitosis and meiosis in maize, suggesting another kinetochore receptor may exist for ZmBub3 (9). This is future work to be explored.

We compared the conserved domains of Knl1 and SAC components between humans and maize and described the architecture of plant Knl1 and SAC signaling based on current and previous findings (Fig. 7). The presence of a kinase domain in maize Bmf1 suggests that this protein has a phosphorylation function; indeed, Bmf1 functions in the phosphorylation of histone H2A in rice and maize (9, 48). Furthermore, the canonical Bub3-binding GLEBS domains have been lost in all plant BMF proteins, indicating that these proteins do not interact with Bub3, as confirmed by Y2H in this study (*SI Appendix*, Fig. S3*B*). The cell-cycle–dependent kinetochore localization of Bub3 signals has been observed during mitosis and meiosis in maize (9), which is a classical feature of the SAC signaling. However, of the three Bub3 homologs in *Arabidopsis*, none localized on the kinetochore (29). No interaction between Knl1 and Bub3 was detected in maize, raising the question of how maize Bub3 is recruited to the kinetochore. The plant BMF proteins both contain the TPR domain as in humans, whereas not all of the BMF proteins retained the interaction with Knl1, and even different mechanisms were adopted for the interaction of Knl1 with the retained BMF protein in plant lineages. The BMF recruitment region in maize Knl1 shows considerable variation in the eudicots that we examined, suggesting that distinct kinetochore architectures are present in different plant species. These results shed light on this intriguing protein in plants and establish a paradigm of divergence and conservation between rapidly evolving kinetochore partners during evolution.

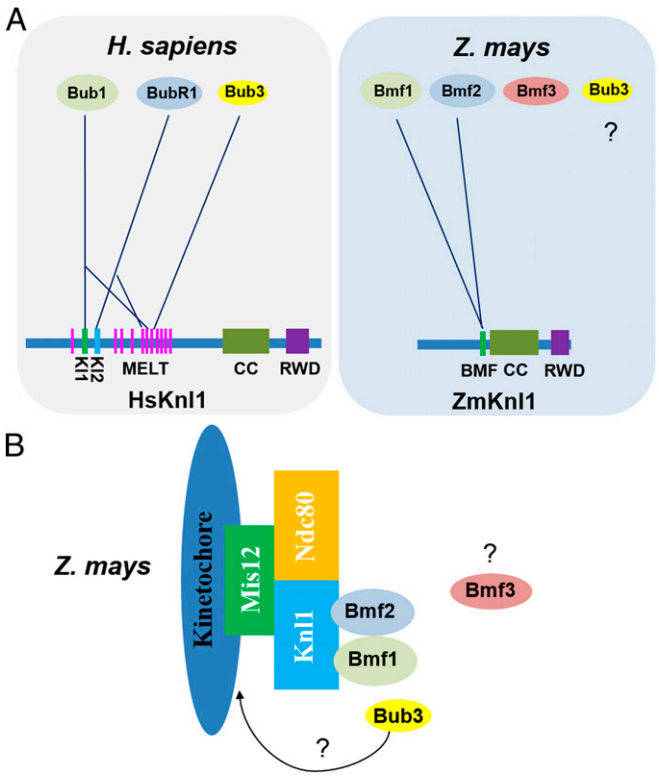

Fig. 7. Models of the architecture of Knl1 with SAC signaling in humans and plants. (*A*) Comparison of the domains of Knl1 proteins and the architecture with SAC signaling between humans (*H. sapiens*) and maize (*Z. mays*). In humans, Knl1 MELT repeats cooperate with KI motifs to recruit SAC signals (Bub1, BubR1, and Bub3). In maize, the MELT repeats of Knl1 are lost, and a 145 aa region in the middle of Knl1 participates in interaction with Bmf1 and Bmf2 in maize. However, no interaction was detected between Knl1 and Bmf3 or Bub3. Different-colored rectangles on Knl1 represent the MELT, KI1, KI2, BMF (BMF-binding domain), coiled-coil (CC), and RWD domain. The solid lines represent detected interaction with the Y2H system. (*B*) Cell-cycle–dependent kinetochore localizations of Bmf1 and Bub3 were detected in maize, a typical feature of SAC signaling. The TPR domains of Bmf1 and Bmf2 are required for their interaction with Knl1. How Bub3 is recruited to the kinetochore and the role of Bmf3 in maize remains unknown.

Materials and Methods

Plant Materials and Growth Conditions. All maize (*Zea mays* L.) plants used in this study were grown in a greenhouse or in the field. Root tips and pollen mother cells from various lines were used for cytological analysis. The *Knl1* Uniform Mu mutant line *UFMu-06469* were kindly provided by the Maize Genetics Cooperation Stock Center (University of Illinois).

Cloning Full-Length Knl1 Complementary DNA (cDNA) and RT-PCR Analysis. Total RNA was isolated from young leaf tissue of the B73 inbred line using TRIzol reagent (Invitrogen). cDNA was synthesized from 2 μg total RNA template via reverse transcription using random primers. Specific primer pairs were used to amplify full-length *ZmKnl1* cDNA (Dataset S4). The PCR amplification products were cloned into the pEASY vector (TransGen Biotech Co., Ltd.) and confirmed by Sanger sequencing. For RT-PCR, total RNA was harvested from various tissues, as mentioned above, and 2 μg total RNA was used for cDNA synthesis. The expression levels of *ZmKnl1* in different tissues were measured by RT-PCR, with *Actin* used as the control gene.

Y2H Assays and Plasmid Constructs. The Y2H assay was performed according to the manufacturer's instructions using plasmids pGBKT7 and pGADT7 (Matchmaker Two-Hybrid System, Clontech Laboratories Inc., Catalog No. 630445). The constructs were transformed into the yeast strain AH109. All the cDNA fragments used were amplified by PCR using specific primer pairs (Dataset S4). Point mutations were introduced into pGBKT7-ZmBmf1, pGBKT7-ZmBmf2, and pGAD-ZmKnl1-M8 by site-directed mutagenesis (Tiangen Biotech Co., Ltd., Catalog No. KM101). The sequences of all plasmid vectors were verified by DNA sequencing. All plasmid clones were prepared for sequence analysis using a TIANprep Mini Plasmid Kit according to the manufacturer's instructions (Tiangen Biotech Co., Ltd, Category No. DP103). The bacterial strain DH5α (*Escherichia coli*) was used for conventional cloning.

Luciferase Complementation Image Assay (LCI). The constructs of ZmBmf1/2-NLUC and ZmKnl1-M8-CLUC were performed using EasyGeno Assembly Cloning kit (Tiangen Biotech Co., Ltd.). The LCI assay was adopted from a previous method (53). The luciferase images were captured using the low-light–cooled, charge-coupled device imaging apparatus (NightOWL II LB983, Berthold Technologies). At least three independent repetitions were performed for each experiment.

Protein Annotation, Sequence Alignment, and Phylogenetic Analysis. The coiled-coil domain was predicted using the tool available at the Pole Bioinformatique Lyonnais website (https://prabi.ibcp.fr/htm/site/web/home). The protein disorder tendency of ZmKnl1 was predicted with FoldIndex (54). The hydropathicity of amino acid was predicated with ProtScale tool with Hphob./Kyte and Doolittle profile (55). The protein structure prediction was performed with the Raptorx server (44).

The Knl1 genes in plants were detected using the NCBI protein database with BLAST or the HMM profiles. The HMM profiles were constructed from the full-length alignment and separate profiles with well-annotated domains (36). Multiple alignments of full-length Knl1 protein sequences from different species were performed using Multiple Sequence Alignment Program with default parameters (56). The alignment results without gaps were used for generating the phylogenetic tree with IQ-Tree software using the maximum likelihood method based on the JTT+F+R4 model (57). The display, annotation, and management of the phylogenetic tree were constructed with Interactive Tree of Life (58). The accession numbers of ZmBmf1, ZmBmf2, ZmBmf3, and ZmBub3 are XP_008650955, XP_008681224, XP_008662383, EU971378.1, and NP_001149777, respectively.

Antibody Production. To generate anti-ZmKnl1 antibodies, peptides corresponding to the C terminus of ZmKnl1 (RKGNAGRRDGDEATRS) were generated. The peptides used to raise maize anti-ZmNdc80 and anti-ZmMis12 antibodies were described previously (34). Keyhole limpet hemocyanin–conjugated

peptides were injected into rabbits, mice, and guinea pigs. The anti-ZmKnl1, anti-ZmNdc80, and anti-ZmMis12 polyclonal antibodies were affinity purified using peptides conjugated to SulfoLink Coupling Resin provided by GL Biochem. The mouse monoclonal anti-tubulin antibody was obtained from MilliporeSigma (Catalog No. DAM1501783). The anti-ZmBmf1 antibody was described previously (9).

Genotyping of Maize Mu Mutants. Genomic DNA was extracted from various maize lines using the CTAB method (59). The ZmKnl1 homozygous Mu mutants were genotyped using the primer pair Knl1-F/Knl1-R (Dataset S1). Primer pair Knl1-F/Knl1-R produced a 1,314 bp band in the WT; primer pair Knl1-R/Mu-TIR produced a single band of ~1,128 bp in the ZmKnl1 homozygous mutant.

Agrobacterium-Mediated Maize Transformation. A high-efficiency DPC CRISPR/Cas9–mediated genome editing system for targeted editing of ZmKnl1 was designed as described (45). Maize Hi-II seeds were planted in the field, and the immature embryos were used for *Agrobacterium*-mediated transformation, as previously described (60). Tissue culture was performed in growth chambers in the dark. Regenerated plants were grown in growth chambers under a 16 h light/8 h dark cycle at 25 °C. The primer pair Cas9-F/Cas9-R (Dataset S4) was used to identify positive transgenic plants. For the PCR-RE assay, ~500 ng purified PCR product per sample covering the target site was digested with *Pvu*-II (New England Biolabs).

Immunolocalization and Image Processing. Root-tip and pollen mother cell tissues were fixed in 4% formaldehyde for 2 h and washed three times with 1× phosphate-buffered saline solution. Immunostaining of mitotic and meiotic cells was performed as described (61) using maize monoclonal antibodies against ZmKnl1, ZmNdc80, ZmMis12, ZmBmf1, and alpha tubulin, as mentioned above. The samples were observed by confocal microscopy (Zeiss Cell Observer SD), and the images were processed with ZEN 2009 Light Edition (Zeiss) and Adobe Photoshop CS 6.0.

RNA Extraction and RNA-Seq. Total RNA was extracted from *zmknl1* or WT kernels from 14 DAP (10 to 20 kernels per sample) using TRIzol reagent. The seed coat was removed from each seed, and two independent biological replicates from different ears were used for analysis. The cDNA libraries were constructed following standard Illumina protocols and sequenced on the Illumina HiSEq. 2500 platform by Berry Genomics Co. Ltd. Sequencing reads were trimmed using Trimmomatic (version 0.36) (62) and mapped to the B73 RefGen_version 3.31 sequence using hisat2 (version 2.0.1 beta) (63). HTseq-count was used to count the reads of all annotated genes (64). Significant DEGs were identified using the DESeq2 package (65) with the thresholds $q\text{-value} < 0.05$ and log2 (fold change) > 1.5. GO annotation was performed using web-based agriGO version 2.0 (66). Semantic similarity-based scatter plots of the functionally enriched GO terms in the biological processes category were produced using REViGO (67) (revigo.irb.hr/).

Data Availability. The RNA-Seq data sets have been submitted to the NCBI Gene Expression Omnibus under accession number GSE124245. All other study data are included in the article and/or supporting information.

ACKNOWLEDGMENTS. We thank Prof. Ingo Schubert from the Leibniz Institute of Plant Genetics and Crop Plant Research and Prof. Gregory P. Copenhaver from the University of North Carolina at Chapel Hill for critical reading of the manuscript and helpful comments. We thank Prof. Jianmin Zhou (Institute of Genetics and Developmental Biology, Chinese Academy of Sciences) for the technical assistance with the LCI assay. This work was supported by the National Natural Science Foundation of China (31630049 and 31920103006).

1. M. R. Przewloka, D. M. Glover, The kinetochore and the centromere: A working long distance relationship. *Annu. Rev. Genet.* **43**, 439–465 (2009).
2. K. M. Godek, L. Kabeche, D. A. Compton, Regulation of kinetochore-microtubule attachments through homeostatic control during mitosis. *Nat. Rev. Mol. Cell Biol.* **16**, 57–64 (2015).
3. I. M. Cheeseman, The kinetochore. *Cold Spring Harb. Perspect. Biol.* **6**, a015826 (2014).
4. A. Petrovic *et al*., Structure of the MIS12 complex and molecular basis of its interaction with CENP-C at human kinetochores. *Cell* **167**, 1028–1040.e15 (2016).
5. R. Ladurner, A. F. Straight, MIS12/MIND control at the kinetochore. *Cell* **167**, 889–891 (2016).
6. I. A. Drinnenberg, S. Henikoff, H. S. Malik, Evolutionary turnover of kinetochore proteins: A ship of theseus? *Trends Cell Biol.* **26**, 498–510 (2016).
7. E. A. Foley, T. M. Kapoor, Microtubule attachment and spindle assembly checkpoint signalling at the kinetochore. *Nat. Rev. Mol. Cell Biol.* **14**, 25–37 (2013).
8. A. Musacchio, E. D. Salmon, The spindle-assembly checkpoint in space and time. *Nat. Rev. Mol. Cell Biol.* **8**, 379–393 (2007).
9. H. Su *et al*., Dynamic location changes of Bub1-phosphorylated-H2AThr133 with CENH3 nucleosome in maize centromeric regions. *New Phytol.* **214**, 682–694 (2017).
10. J. J. van Hooff, E. Tromer, L. M. van Wijk, B. Snel, G. J. Kops, Evolutionary dynamics of the kinetochore network in eukaryotes as revealed by comparative genomics. *EMBO Rep.* **18**, 1559–1571 (2017).
11. V. S. Nekrasov, M. A. Smith, S. Peak-Chew, J. V. Kilmartin, Interactions between centromere complexes in Saccharomyces cerevisiae. *Mol. Biol. Cell* **14**, 4931–4946 (2003).
12. A. Desai *et al*., KNL-1 directs assembly of the microtubule-binding interface of the kinetochore in C. elegans. *Genes Dev.* **17**, 2421–2435 (2003).
13. I. M. Cheeseman, T. Hori, T. Fukagawa, A. Desai, KNL1 and the CENP-H/I/K complex coordinately direct kinetochore assembly in vertebrates. *Mol. Biol. Cell* **19**, 587–594 (2008).
14. I. M. Cheeseman *et al*., A conserved protein network controls assembly of the outer kinetochore and its ability to sustain tension. *Genes Dev.* **18**, 2255–2268 (2004).
15. T. Kiyomitsu, C. Obuse, M. Yanagida, Human Blinkin/AF15q14 is required for chromosome alignment and the mitotic checkpoint through direct interaction with Bub1 and BubR1. *Dev. Cell* **13**, 663–676 (2007).
16. T. Kiyomitsu, H. Murakami, M. Yanagida, Protein interaction domain mapping of human kinetochore protein Blinkin reveals a consensus motif for binding of spindle assembly checkpoint proteins Bub1 and BubR1. *Mol. Cell. Biol.* **31**, 998–1011 (2011).
17. V. Silió, A. D. McAinsh, J. B. Millar, KNL1-Bubs and RZZ provide two separable pathways for checkpoint activation at human kinetochores. *Dev. Cell* **35**, 600–613 (2015).
18. G. V. Caldas, J. G. DeLuca, KNL1: Bringing order to the kinetochore. *Chromosoma* **123**, 169–181 (2014).
19. V. M. Bolanos-Garcia *et al*., Structure of a Blinkin-BUBR1 complex reveals an interaction crucial for kinetochore-mitotic checkpoint regulation via an unanticipated binding site. *Structure* **19**, 1691–1700 (2011).
20. V. Krenn, A. Wehenkel, X. Li, S. Santaguida, A. Musacchio, Structural analysis reveals features of the spindle checkpoint kinase Bub1-kinetochore subunit Knl1 interaction. *J. Cell Biol.* **196**, 451–467 (2012).
21. Y. Yamagishi, C.-H. Yang, Y. Tanno, Y. Watanabe, MPS1/Mph1 phosphorylates the kinetochore protein KNL1/Spc7 to recruit SAC components. *Nat. Cell Biol.* **14**, 746–752 (2012).
22. N. London, S. Ceto, J. A. Ranish, S. Biggins, Phosphoregulation of Spc105 by Mps1 and PP1 regulates Bub1 localization to kinetochores. *Curr. Biol.* **22**, 900–906 (2012).
23. L. A. Shepperd *et al*., Phosphodependent recruitment of Bub1 and Bub3 to Spc7/KNL1 by Mph1 kinase maintains the spindle checkpoint. *Curr. Biol.* **22**, 891–899 (2012).
24. I. Primorac *et al*., Bub3 reads phosphorylated MELT repeats to promote spindle assembly checkpoint signaling. *eLife* **2**, e01030 (2013).
25. V. Krenn, K. Overlack, I. Primorac, S. van Gerwen, A. Musacchio, KI motifs of human Knl1 enhance assembly of comprehensive spindle checkpoint complexes around MELT repeats. *Curr. Biol.* **24**, 29–39 (2014).
26. E. Tromer, B. Snel, G. J. P. L. Kops, Widespread recurrent patterns of rapid repeat evolution in the kinetochore scaffold KNL1. *Genome Biol. Evol.* **7**, 2383–2393 (2015).
27. I. Lermontova, J. Fuchs, I. Schubert, The Arabidopsis checkpoint protein Bub3.1 is essential for gametophyte development. *Front. Biosci.* **13**, 5202–5211 (2008).
28. M.-C. Caillaud *et al*., Spindle assembly checkpoint protein dynamics reveal conserved and unsuspected roles in plant cell division. *PLoS One* **4**, e6757 (2009).
29. S. Komaki, A. Schnittger, The spindle assembly checkpoint in Arabidopsis is rapidly shut off during severe stress. *Dev. Cell* **43**, 172–185.e5 (2017).
30. S. Komaki, A. Schnittger, The spindle checkpoint in plants-a green variation over a conserved theme? *Curr. Opin. Plant Biol.* **34**, 84–91 (2016).
31. H. Zhang *et al*., Role of the BUB3 protein in phragmoplast microtubule reorganization during cytokinesis. *Nat. Plants* **4**, 485–494 (2018). Correction in: *Nat. Plants* **4**, 731 (2018).
32. S. Elowe, Bub1 and BubR1: At the interface between chromosome attachment and the spindle checkpoint. *Mol. Cell. Biol.* **31**, 3085–3093 (2011).
33. Y. Du, R. K. Dawe, Maize NDC80 is a constitutive feature of the central kinetochore. *Chromosome Res.* **15**, 767–775 (2007).
34. X. Li, R. K. Dawe, Fused sister kinetochores initiate the reductional division in meiosis I. *Nat. Cell Biol.* **11**, 1103–1108 (2009).
35. E. Kozgunova, M. Nishina, G. Goshima, Kinetochore protein depletion underlies cytokinesis failure and somatic polyploidization in the moss *Physcomitrella patens*. *eLife* **8**, e43652 (2019).
36. E. C. Tromer, J. J. E. van Hooff, G. J. P. L. Kops, B. Snel, Mosaic origin of the eukaryotic kinetochore. *Proc. Natl. Acad. Sci. U.S.A.* **116**, 12873–12882 (2019).
37. S. F. Altschul, W. Gish, W. Miller, E. W. Myers, D. J. Lipman, Basic local alignment search tool. *J. Mol. Biol.* **215**, 403–410 (1990).
38. D. A. Benson *et al*., GenBank. *Nucleic Acids Res.* **43**, D30–D35 (2015).
39. Amborella Genome Project, The Amborella genome and the evolution of flowering plants. *Science* **342**, 1241089 (2013).
40. M. Vleugel *et al*., Sequential multisite phospho-regulation of KNL1-BUB3 interfaces at mitotic kinetochores. *Mol. Cell* **57**, 824–835 (2015).
41. L. D. D'Andrea, L. Regan, TPR proteins: The versatile helix. *Trends Biochem. Sci.* **28**, 655–662 (2003).
42. V. M. Bolanos-Garcia, T. L. Blundell, BUB1 and BUBR1: Multifaceted kinases of the cell cycle. *Trends Biochem. Sci.* **36**, 141–150 (2011).

43. V. M. Bolanos-Garcia *et al*., The crystal structure of the N-terminal region of BUB1 provides insight into the mechanism of BUB1 recruitment to kinetochores. *Structure* **17**, 105–116 (2009).
44. S. Wang, W. Li, S. Liu, J. Xu, RaptorX-property: A web server for protein structure property prediction. *Nucleic Acids Res.* **44**, W430–W435 (2016).
45. C. Feng *et al*., High-efficiency genome editing using a dmc1 promoter-controlled CRISPR/Cas9 system in maize. *Plant Biotechnol. J.* **16**, 1848–1857 (2018).
46. F. Feng *et al*., OPAQUE11 is a central hub of the regulatory network for maize endosperm development and nutrient metabolism. *Plant Cell* **30**, 375–396 (2018).
47. Y. Huang *et al*., Maize VKS1 regulates mitosis and cytokinesis during early endosperm development. *Plant Cell* **31**, 1238–1256 (2019).
48. M. Wang *et al*., BRK1, a Bub1-related kinase, is essential for generating proper tension between homologous kinetochores at metaphase I of rice meiosis. *Plant Cell* **24**, 4961–4973 (2012).
49. G. J. P. L. Kops, B. Snel, E. C. Tromer, Evolutionary dynamics of the spindle assembly checkpoint in eukaryotes. *Curr. Biol.* **30**, R589–R602 (2020).
50. H. J. Dyson, P. E. Wright, Intrinsically unstructured proteins and their functions. *Nat. Rev. Mol. Cell Biol.* **6**, 197–208 (2005).
51. P. Tompa, Intrinsically disordered proteins: A 10-year recap. *Trends Biochem. Sci.* **37**, 509–516 (2012).
52. C. J. Brown, A. K. Johnson, A. K. Dunker, G. W. Daughdrill, Evolution and disorder. *Curr. Opin. Struct. Biol.* **21**, 441–446 (2011).
53. H. Chen *et al*., Firefly luciferase complementation imaging assay for protein-protein interactions in plants. *Plant Physiol.* **146**, 368–376 (2008).
54. V. N. Uversky, J. R. Gillespie, A. L. Fink, Why are "natively unfolded" proteins unstructured under physiologic conditions? *Proteins* **41**, 415–427 (2000).
55. M. R. Wilkins *et al*., Protein identification and analysis tools in the ExPASy server. *Methods Mol. Biol.* **112**, 531–552 (1999).
56. K. Katoh, D. M. Standley, MAFFT multiple sequence alignment software version 7: Improvements in performance and usability. *Mol. Biol. Evol.* **30**, 772–780 (2013).
57. B. Q. Minh *et al*., IQ-TREE 2: New models and efficient methods for phylogenetic inference in the genomic era. *Mol. Biol. Evol.* **37**, 1530–1534 (2020). Correction in: *Mol. Biol. Evol.* **37**, 2461 (2020).
58. I. Letunic, P. Bork, 20 years of the SMART protein domain annotation resource. *Nucleic Acids Res.* **46** (D1), D493–D496 (2018).
59. N. M. Springer, Isolation of plant DNA for PCR and genotyping using organic extraction and CTAB. *Cold Spring Harb. Protoc.* **2010**, pdb prot5515 (2010).
60. C. Feng *et al*., Efficient targeted genome modification in maize using CRISPR/Cas9 system. *J. Genet. Genomics* **43**, 37–43 (2016).
61. F. Han, J. C. Lamb, W. Yu, Z. Gao, J. A. Birchler, Centromere function and nondisjunction are independent components of the maize B chromosome accumulation mechanism. *Plant Cell* **19**, 524–533 (2007).
62. A. M. Bolger, M. Lohse, B. Usadel, Trimmomatic: A flexible trimmer for Illumina sequence data. *Bioinformatics* **30**, 2114–2120 (2014).
63. D. Kim, B. Langmead, S. L. Salzberg, HISAT: A fast spliced aligner with low memory requirements. *Nat. Methods* **12**, 357–360 (2015).
64. S. Anders, P. T. Pyl, W. Huber, HTSeq–A Python framework to work with high-throughput sequencing data. *Bioinformatics* **31**, 166–169 (2015).
65. M. I. Love, W. Huber, S. Anders, Moderated estimation of fold change and dispersion for RNA-seq data with DESeq2. *Genome Biol.* **15**, 550 (2014).
66. T. Tian *et al*., agriGO v2.0: A GO analysis toolkit for the agricultural community, 2017 update. *Nucleic Acids Res.* **45**, W122–W129 (2017).
67. F. Supek, M. Bošnjak, N. Škunca, T. Šmuc, REVIGO summarizes and visualizes long lists of gene ontology terms. *PLoS One* **6**, e21800 (2011).